Sum Frequency Generation Vibrational Spectra: The Influence of Experimental Geometry for an Absorptive Medium or Media

Roger L. York,[†,‡] Yimin Li,[†] George J. Holinga,[†] and Gabor A. Somorjai*[†]

Department of Chemistry, University of California, Berkeley, California 94720, and Materials Science Division, Lawrence Berkeley National Laboratories, Berkeley, California 94720

Received: September 29, 2008; Revised Manuscript Received: January 9, 2009

The influence of experimental geometry on infrared total internal reflection surface sum frequency generation (SFG) vibrational spectra at the water/solid interface has been examined. A detailed analysis of the experimental geometry revealed that the enhancement of SFG signal for the "critical angle" can be much weaker than previously thought if the index of refraction of the transmitted or reflected medium is treated as a complex value (i.e., the imaginary part of the index of refraction is not zero and not neglected). The theoretical analysis outlined here agreed well with the experimental results of the SFG spectra of the silica/water interface in two different geometries. This paper deals with the *SSP* polarization combination.

1. Introduction

SFG vibrational spectroscopy was first developed in 1987.[1−3] It has expanded over the last 20 years to become a common and well-established technique in surface characterization and study, showing exceptional potential for the study of buried interfaces.[4−36] It has long been understood that the angles of incidence of the visible and infrared (IR) beams influence the intensity of the SFG signal. If the IR or visible light is at the critical angle, then the resultant SFG signal can be enhanced. This total internal reflection SFG (TIR-SFG) has been shown to be a promising technique for obtaining SFG spectra when the SFG signal is weak. First demonstrated by Hatch et al. in 1992,[37] this technique is now used by several groups.[38−57] Although the benefits of using TIR-SFG are clear, the interpretation of infrared TIR-SFG spectra can be complicated, especially at the water/solid interface.[6,10] This is due to the fact that the index of refraction of water undergoes a significant change (∼25%) as the infrared is tuned over the spectral region of interest spanning 2800−3600 cm^{-1}.[58]

In this report, we examine the influence of the angles of incidence of the visible and infrared (IR) beam on the intensity of surface-specific IR−visible sum frequency generation (SFG) vibrational spectroscopy signal at the interface between absorptive media. We show that if the index of refraction of the transmitted and/or reflected medium is complex (i.e., not a real value), then the nonlinear Fresnel coefficients (which describe the ratio of the intensity of incident to reflected light) can be markedly different than the case in which the index of refraction is purely real. This is true even if the imaginary part of the index of refraction is a small fraction of the real part of the index of refraction. We explore the implications of this observation by comparing the experimental and theoretical SFG spectra of the silica/water interface at two different geometries.

In one of the possible geometries for TIR-SFG at the water/solid interface, the incident angle of the IR light is very close to the critical angle of total internal reflection, while the incident angle of the visible light is far away from the critical angle (hereby, we refer to this geometry as the IR TIR-SFG). The common belief is that this geometry may significantly enhance the IR Fresnel coefficient and increase the intensity of the SFG signal. In this report, we show that this common belief is not valid when the IR is scanned over a frequency region where water is absorptive. From our theoretical analysis, we further show that the enhancement of the IR Fresnel coefficient for this geometry is frequency dependent, which may change the intensity ratio of measured SFG peaks in different frequency region. Our findings explain why visible TIR-SFG (namely, keeping the visible light at the critical angle and IR light far from the critical angle) is the better geometry for the SFG studies at the water/solid interface.[59]

2. Theoretical Analysis

In vibrational SFG, a visible beam at 532 nm (ω_{VIS}) is mixed with a tunable (here 2800−3600 cm^{-1}) IR beam (ω_{IR}) to produce a coherent beam at the sum frequency of the two incoming beams (ω_{SFG}). The intensity of this the light at the sum frequency (I_{SFG}) is measured as a function of ω_{IR}. I_{SFG} is proportional to the square of the macroscopic second-order hyperpolarizability, $\chi^{(2)}$, which contains the relevant chemical information about the interfacial adsorbates.[1−3]

The purpose of this paper is to understand the origin of enhancement of SFG intensity by changing geometries and the possible complexity associated with this due to the frequency-dependent complex index of refraction of water in the IR frequency region of interest. To the best of our knowledge, there are no publications that have explicitly treated an absorptive medium or media in the SFG intensity calculation. The SFG intensity formula for a thin film model (or three-layer model shown in Figure 1) in which the refraction indices of three layers can be complex gives this final result for the $S_{SFG}S_{VIS}P_{IR}$ polarization combination[60,61]

* To whom correspondence should be addressed. E-mail: somorjai@berkeley.edu.
† These authors contributed equally to this work.
‡ Current address: Department of Chemistry and Chemical Biology, Harvard University.

10.1021/jp808629r CCC: $40.75 © 2009 American Chemical Society
Published on Web 02/24/2009

$$I_{ssp}^{SFG} = \frac{32\pi^3\omega_s^2}{c^3}\frac{\mathrm{Re}[\varepsilon_1^{1/2}(\omega_s)]}{|\varepsilon_1(\omega_s)|\mathrm{Re}[\varepsilon_1^{1/2}(\omega_{Vis})\varepsilon_1^{1/2}(\omega_{IR})]} \times \left|\chi_{yyz}^{(2)}(\omega_s)\sec\beta\sin\beta_{IR}L^S L_T^{Vis} L_T^{IR}\frac{\varepsilon_1^{1/2}(\omega_{IR})\varepsilon_2^{1/2}(\omega_{IR})}{\varepsilon_M(\omega_{IR})}\right|^2 I^{Vis} I^{IR} \quad (1)$$

where

$$L^S = \frac{2\varepsilon_1^{1/2}(\omega_s)\cos\beta}{\varepsilon_2^{1/2}(\omega_s)\cos\gamma + \varepsilon_2^{1/2}(\omega_s)\cos\beta} \quad (2)$$

$$L_T^{Vis} = \frac{2\varepsilon_2^{1/2}(\omega_{Vis})\cos\beta_{Vis}}{\varepsilon_2^{1/2}(\omega_{Vis})\cos\gamma_{Vis} + \varepsilon_1^{1/2}(\omega_{Vis})\cos\beta_{Vis}} \quad (3)$$

$$L_T^{IR} = \frac{2\varepsilon_1^{1/2}(\omega_{IR})\cos\beta_{IR}}{\varepsilon_2^{1/2}(\omega_{IR})\cos\beta_{IR} + \varepsilon_1^{1/2}(\omega_{IR})\cos\gamma_{IR}} \quad (4)$$

The various angles and dielectric constants in eq 1 are shown in Figure 1. L^S, L_T^{Vis} and L_T^{IR} are Fresnel's coefficients of the transmitted sum frequency, visible, and IR light in medium 2, respectively.

In an SFG experiment, one measures the SFG intensity, $I^{SFG}(\omega_{IR})$, as a function of the IR frequency and then extracts the frequency dependency of $|\chi^{(2)}(\omega_{IR})|^2$. This gives the molecular-level information about the interface. However, in order to directly correlate $|\chi^{(2)}(\omega_{IR})|^2$ with $I^{SFG}(\omega_{IR})$, we must assume that all the factors other than $|\chi^{(2)}(\omega_{IR})|^2$ in eq 1 do not significantly vary with the IR frequency. This assumption can fail in several different circumstances. For example, in the case where medium 1 is absorptive to IR, the IR beam may be partially absorbed by the bulk of medium 1. Hence, the intensity of IR light, I^{IR}, reaching the interface may vary with the IR frequency. Even if this intensity variation can be suppressed by using a sufficiently thin layer of medium 1, the effect of the frequency dependence of $\varepsilon_1(\omega_{IR})$ and $L_T^{IR}(\omega_{IR})$ still needs to be carefully considered.

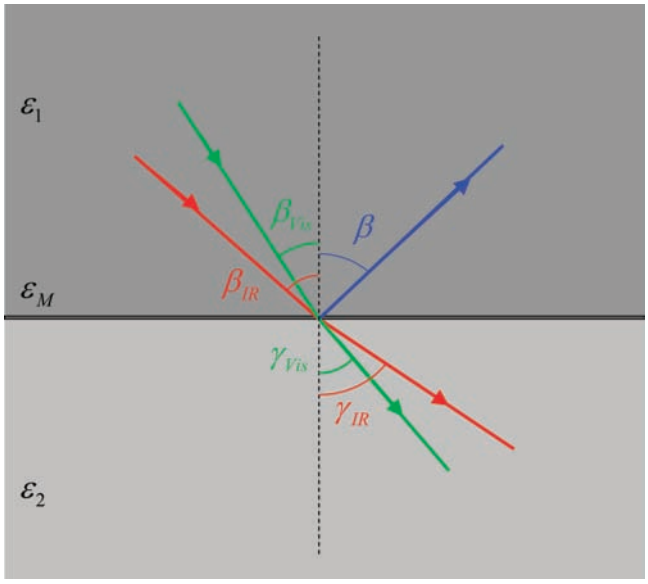

Figure 1. SFG diagram showing the various angles and dielectric constants in eq 1.

Here we mainly focus on the water/silica interface where medium 2, water, has an absorption band over the frequency region of interest and show how the absorptive nature of water can affect the IR TIR-SFG intensity in the s-polarized sum frequency, s-polarized visible, and p-polarized infrared (ssp) polarization combination. In order to experimentally confirm the results of our theoretical analysis, we performed SFG experiments in two different geometries. In order to minimize uncertainty in the angles of incidence, the angles of incidence with respect to the sample surface normal were not changed by moving optics. Rather, two different silica substrates were used to change how light refracts into the substrate, as shown in Figure 2. These two substrates were a fused silica slab (hereby called "slab") and a fused silica prism (hereby called "prism"). The resultant angles of incidence are given in Table 1.

To see the influence of geometry on the SFG intensity, we define a dimensionless geometric factor $G(\beta_{Vis},\beta_{IR})$ as

$$G(\beta_{Vis},\beta_{IR}) = |\sec\beta\sin\beta_{IR}L^S L_T^{Vis} L_T^{IR}|^2 \quad (5)$$

This factor includes all terms in the SFG intensity expression that depend on incident angles, β_{Vis} and β_{IR}. From eq 1, we can see that the ratio between two geometric factors for two geometries is equal to the ratio of the SFG intensity for the two geometries, $I_{prism}^{SFG}/I_{slab}^{SFG} = G_{prism}/G_{slab}$. This ratio is independent of the nonlinear susceptibility, $\chi_{yyz}^{(2)}$, so it is a good quantity for studying the effects induced by geometry change.

To understand the origin of the SFG intensity changes due to the different geometries, we performed simulations of the ratio of the ssp SFG intensities for two geometries. In the simulations, the refractive index of silica, $\varepsilon_1^{1/2}$, is equal to 1.46 for the visible light and the SFG light and 1.41 for the IR light. For the visible light and SFG light, the refractive index of water, $\varepsilon_1^{1/2}$, is equal to 1.34, while for IR light in the region from 2800 to 3600 cm^{-1}, the refractive index of water is a function of the IR frequency obtained from a fitting of experimental data[58] (see Figure A.1). Since we do not know the refractive index of the thin film, we set $\varepsilon_M^{1/2}$ to be 1.40 for visible light and 1.38 for IR light. However, from eq 1, we can see that the ratio of SFG intensities, $I_{prism}^{SFG}/I_{slab}^{SFG}$, does not depend on $\varepsilon_M^{1/2}$.

Figure 3a shows the G factors at three IR frequencies as a function of the average of two incident angles, $(\beta_{IR} + \beta_{Vis})/2$, with the difference, $\beta_{IR} - \beta_{Vis}$, fixed to 6°. Figure 3a shows the trends of the SFG intensity enhancement (or the increase of G) when the incident angles become close to the TIR limits, and the extent of enhancement at different IR frequencies can be quite different.

The geometric factor depends on the IR frequency because L_T^{IR} in eq 5 is a function of the frequency-dependent refractive index of water. Figure 3b shows the IR-frequency dependence of G_{prism}/G_{slab}. For the prism geometry, the frequency dependence is quite prominent. Thus, caution must be taken when making quantitative analysis of the SFG signal from a IR-TIR-SFG experiment, since the frequency dependence of the SFG signal is coming from not only the second-order susceptibility but also the geometric factor.

To further investigate the origin of the enhancement by the TIR geometry, we first look at the ratios of the Fresnel coefficients ($|L^S|^2$, $|L_T^{Vis}|^2$, and $|L_T^{IR}|^2$) between two geometries in Figure 4a. All these ratios are less than 1.3, so these Fresnel coefficients do not contribute much to the enhancement of the SFG intensity. In our prism geometry, the incident angle of the visible light (~57°) is still far away from the critical angle for

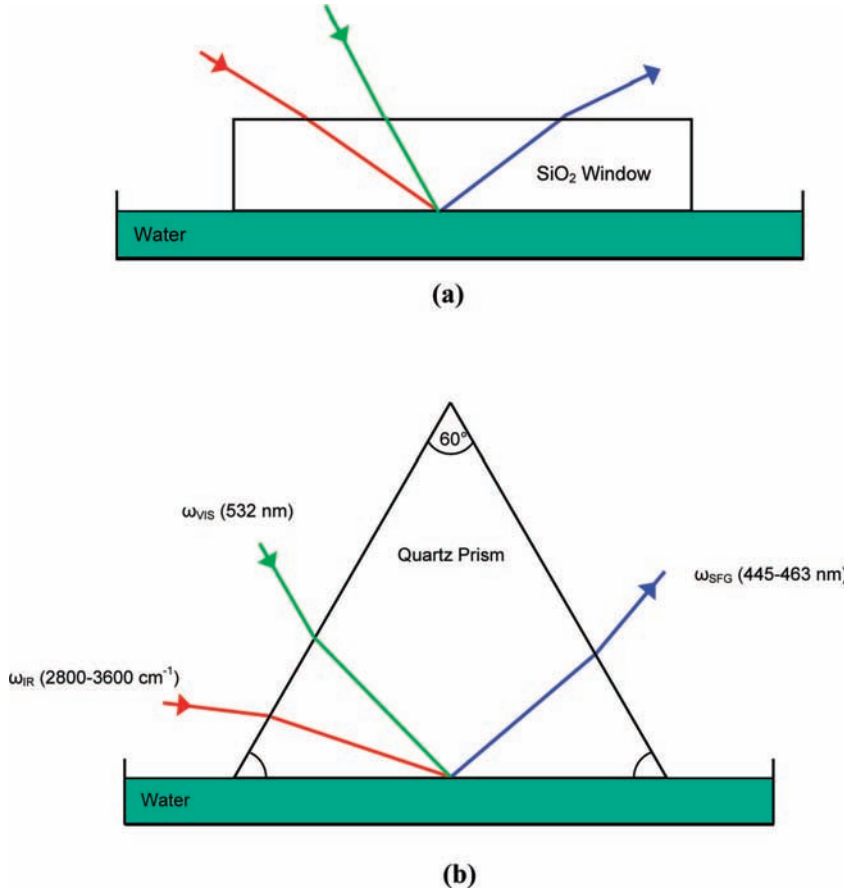

Figure 2. Scheme of the (a) "slab" geometry and (b) "prism" geometry used in this work. See Table 1 for the respective angles of incidence.

TABLE 1: Incident Angles for Different Geometries

geometry	slab	prism
β_{Vis}	36°	57°
β_{IR}	39°	64°

the visible light (~67°), and the SFG light has the reflective angle and frequency very close to the visible light. Thus, the small contribution from the transmitted electrical field of the visible and SFG light is reasonable. However, the incident angle of the IR light in the prism geometry is expected to be very close to the TIR critical angle; thus, it is quite a surprise that the calculated Fresnel coefficient for the prism geometry is less than that for the slab geometry in a large part of the IR frequency region. A detailed analysis in Appendix A shows that this is caused by the frequency-dependent *complex* refractive index of water and the fact that the real part of the water refractive index is quite close to the refractive index of silica.

Figure 4b shows that by changing the geometry from slab to prism, $|\sin \beta_{IR}|^2$ and $|\sec \beta_{SFG}|^2$ are more than doubled. Thus, one reason for the enhancement in our prism geometry is the increase of the projection of the transmitted IR electric field in the z direction, since this projection is proportional to $\sin \beta_{IR}$.

The main source for this frequency dependence comes from the Fresnel coefficient of the IR light which is a function of the frequency-dependent complex refractive index of water. This conclusion is supported by the clear correlation between the frequency dependence of $|L^{IR}_{T,prism}(\omega_{IR})/L^{IR}_{T,slab}(\omega_{IR})|^2$ in Figure 4a and that of $G_{prism}(\omega_{IR})/G_{slab}(\omega_{IR})$ in Figure 3b. This frequency dependence can be eliminated by using the visible TIR-SFG geometry. In this geometry, the enhancement of SFG intensity comes from the Fresnel coefficient of the visible light, and the IR Fresnel coefficient is not sensitive to the frequency change since the incident IR light is far away from the critical angle (see Figure 3a).

3. Experimental Comparisons of Different Geometries

In order to confirm the results of the theoretical analysis provided above, we performed a number of experiments in the two geometries described above (slab and prism). Figure 5 compares the SFG spectra of the polystyrene/air interface[62] in the two geometries. As can be seen, the overall signal is much greater in the prism geometry. Indeed, modes not seen above the noise level in the slab are clearly apparent in the prism geometry.

In order to quantitatively compare experiment with theory, we measured the SFG spectra of the fused silica/pure water (no buffer) interface[10,63] in two geometries as seen in Figure 6. For a quantitative comparison, we subtracted all residual visible intensity from the spectra. The error bars shown are from the average of 5 scans of 200 shots per data point (for the prism) and 8 scans of 200 shots per data point (for the slab). Figure 7 shows a ratio of the intensities of the two geometries (prism/slab) as a function of infrared energy. This quantity should be independent of $\chi^{(2)}$ and only contain geometric variables. This is compared to the ratio of Gs from Figure 3b (prism/slab). The theory agrees reasonably well with the experiment (within the experimental error), showing approximately an order of magnitude increase in signal from slab to prism. Below 2900 cm^{-1}, the theory slightly overestimates the ratio, and above 2900 cm^{-1}, the theory slightly underestimates the ratio. Interestingly, most of the SFG signal below 2900 cm^{-1} is from nonresonant signal, and most of the signal above 2900 cm^{-1} is from resonant enhancement from interfacial water molecules. This may imply

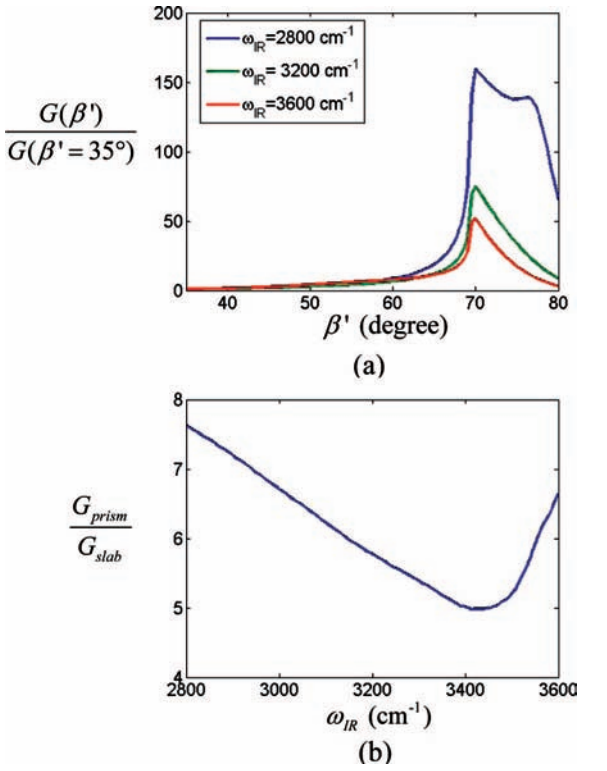

Figure 3. Optical effect of changing geometry on the SFG intensity: (a) the geometric factor $G(\beta_{Vis},\beta_{IR})$ as a function of the average of two incident angles $\beta' = (\beta_{Vis} + \beta_{IR})/2$ with the difference $\beta_{IR} - \beta_{Vis}$ fixed at 6°. The enhancement of the SFG intensities by the TIR geometries is shown for three IR frequencies. The geometric factor has been normalized by the geometric factor with $\beta' = 35°$. (b) IR frequency dependence of the geometric factor for the prism geometry (see Table 1). The geometric factor has been normalized by the geometric factor for the slab geometry.

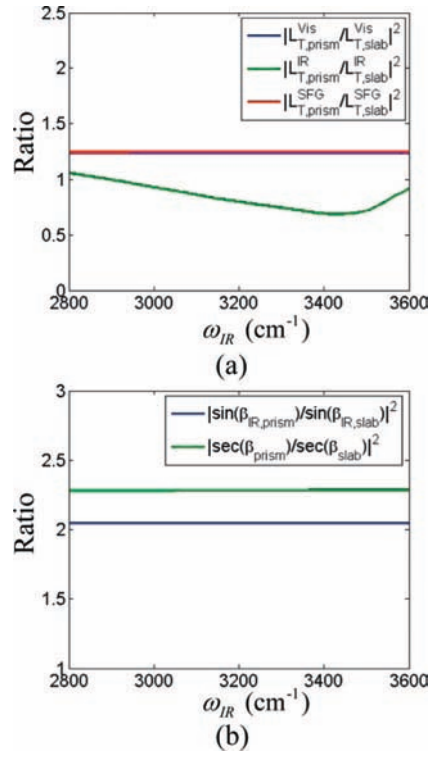

Figure 4. (a) Various ratios of the Fresnel's coefficients between two geometries. All ratios are less than 1.3. The ratio of the Fresnel's coefficient for the IR light has a apparent frequency dependence, while the others for the visible and SFG light do not. (b) Ratios of two angle-related factors $|\sin \beta_{IR}|^2$ and $|\sec \beta|^2$. These ratios are greater than 2 and the main contributors to the enhancement of the SFG intensity when the incident angles are close to the TIR geometry.

that an improved model would need to incorporate local field effects such as dipolar coupling.

4. Conclusions

The influence of an adsorptive medium on the SFG intensity has been studied as a function of angle of incidence of the IR and visible beams. It was observed that if the index of refraction of the transmitted or reflected medium is complex (even if the imaginary part of the index of refraction is small relative to the real part) the Fresnel coefficient can change significantly relative to the situation in which this index of refraction is completely real. This has important consequences for extraction of $\chi^{(2)}$ from the intensity of SFG signal. Therefore, it is concluded that neglecting the imaginary part of the index of refraction (which is unknown for many systems) can introduce error in quantitative analysis of SFG experimental data and should be avoided, especially if the IR beam is near the critical angle.

Appendix A: TIR Geometry of IR Light at the Silica/Water (Adsorptive Medium) Interface

The model in this appendix is of an interface between two dielectric media, medium 1 and medium 2. If the refractive indices are called n_1 and n_2, are all real, and $n_1 > n_2$, there is a critical angle β_c. For incident angles in the close vicinity of β_c the transmitted electric field can be significantly enhanced. The maximum enhancement is given by the Fresnel coefficient of the transmitted field at the critical angle, $L_T(\beta_c) = E_T/E_i = 2n_1/n_2$, where E_T and E_i are the electric fields of the transmitted

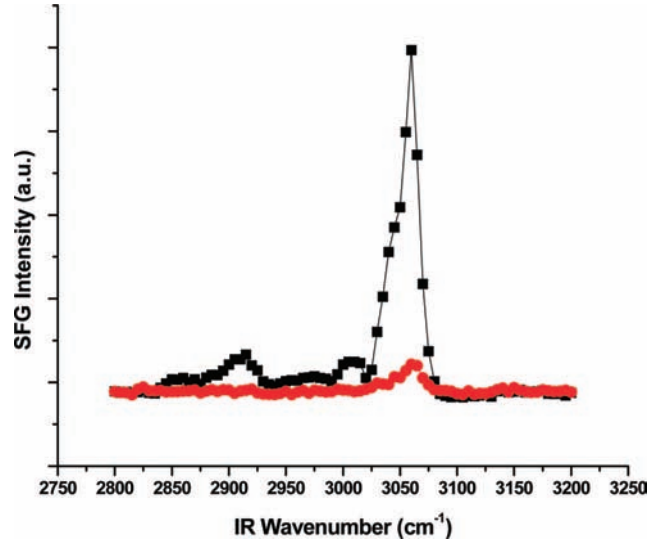

Figure 5. SFG spectra of the polystyrene/air interface in the slab (red circle) and prism (black squares) geometries. Note the increase in the SFG signal in the prism geometry. Additionally, vibrational modes not clearly seen in the slab geometry (due to the low signal-to-noise ratio) are clearly present in the prism geometry (e.g., the mode around 2915 cm^{-1}).

and incident light. The critical angle β_c (also called the total internal reflection (TIR) angle) satisfies $\sin \beta_c = n_2/n_1$. This effect has been used by several research groups to enhance the SFG intensity in their studies of molecular vibrational spectroscopy at interfaces, as mentioned above.

For the silica−water interface, if we take $n_1 = 1.46$ and $n_2 = 1.34$, then the critical angle is about 67°. The IR incident

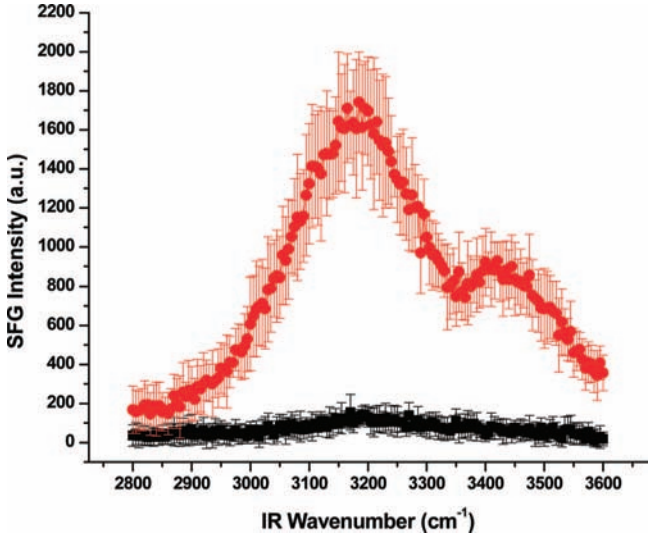

Figure 6. SFG spectra of the pure water/silica interface for both the prism (red circles) and the slab (black squares). Error bars come from the average of 5 scans of 200 shots per data point (for the prism) and 8 scans of 200 shots per data point (for the slab).

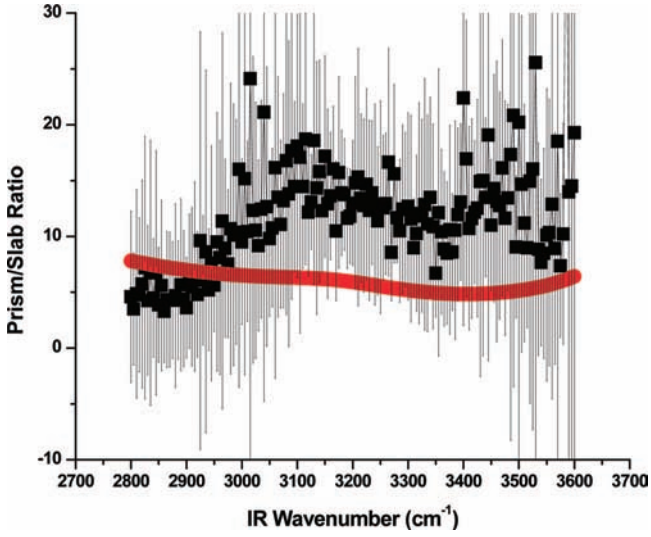

Figure 7. Ratio of the prism geometry to the slab geometry (from Figure 6) is plotted in black squares with associated error bars. The red circles are the ratio of G(prism) to G(slab) (see Figure 3b). The theory shows weak infrared wavelength dependence and approximately an order of magnitude increase in signal from slab to prism. Note that the theory slightly underestimates the magnitude of the increase but is within the experimental error of our measurement.

angle in our near TIR geometry is about 63°, which is quite close to the critical angle. It was expected that the transmitted IR electric field should have a quite significant enhancement. However, Figure 4a shows that, in most of the IR frequency range 2800−3600 cm^{-1}, the ratio $|L^{IR}_{T,prism}/L^{IR}_{T,slab}|^2$ is less than 1.

To explain this observation, we note that water is adsorptive in the IR frequency range of concern. The frequency-dependent complex refractive index of water is shown in Figure A.1. At an IR wavenumber of about 3350 cm^{-1}, the imaginary part of the refractive index can be up to 25% of the real part. Figure A.2 shows that, with the imaginary part of the refractive index increasing, the maximum value of $|L^{IR}_T|^2$ decreases. When the imaginary part of the refractive index is about 9% of the real part, there is almost no enhancement of $|L^{IR}_T|^2$ at the critical angle β_c. In order to answer why a small increase of the imaginary part of the index can have a large influence on $|L^{IR}_T|^2$, we made

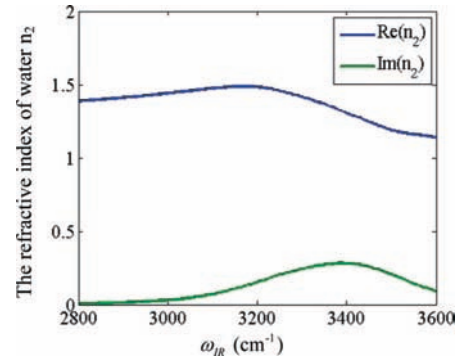

Figure A.1. Refractive index of water in the IR frequency range 2800−3600 cm^{-1}. The imaginary part n_2'' has a maximum at about 3350 cm^{-1}, which is about 25% of the real part n_2'.

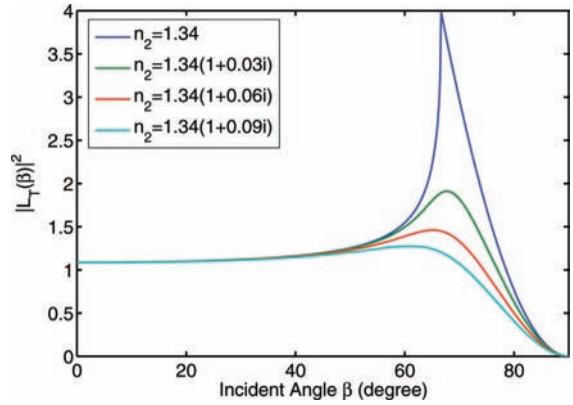

Figure A.2. Effect of the imaginary part of the index of refraction of water on $|L_T(\beta)|^2$ as described in eq 4. The refractive index n_1 is 1.46, and the real part n_2' is 1.34. The imaginary part n_2'' is varying from 0 to 9% of n_2'. The significant decrease of the maximum of $|L_T(\beta)|^2$ is clear even when n_2'' is a small fraction of n_2'.

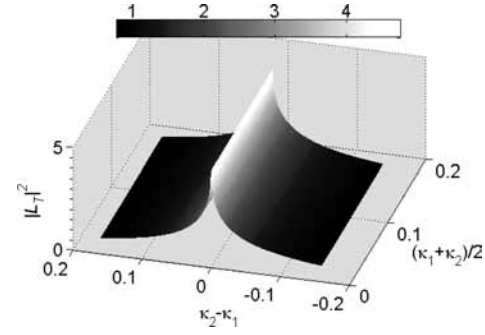

Figure A.3. Effect of the imaginary parts of the index of refraction $n_1 = n_1'(1 + i\kappa_1)$ and $n_2 = n_2'(1 + i\kappa_2)$ on $|L_T(\beta_c^0)|^2$, the Fresnel coefficient at the critical angle described in eq 4. Here n_1' is 1.46, and n_2' is 1.34. $|L_T(\beta_c^0)|^2$ is plotted against $\kappa_2 - \kappa_1$ and $(\kappa_1 + \kappa_2)/2$.

the following analysis based on a small value of the imaginary part of refractive index (relative to the real part). Suppose n_1 is real and $n_2 = n_2'(1 + i\kappa)$, where n_2' is the real part of n_2 and $\kappa = n_2''/n_2'$ is the ratio between the imaginary and the real part of n_2. In the case of $\kappa = 0$, the critical angle β_c^0 satisfies

$$\sin \beta_c^0 = \frac{n_2'}{n_1} \tag{A.1}$$

From Figure A.2, we can see that, with the small increases of κ, the angle β at which $|L_T(\beta)|^2$ reaches its maximum is still

very close to β_c^0. Thus, it seems reasonable to estimate the maximum of $|L_T(\beta)|^2$ by its value at β_c^0.

From Snell's law, we have

$$\sin(\gamma) = \frac{n_1 \sin(\beta_c^0)}{n_2'(1 + i\kappa)} = \frac{1}{1 + i\kappa}$$

For a small $\kappa \ll 1$, it follows that

$$\cos(\gamma) = \sqrt{1 - \left(\frac{1}{1 + i\kappa}\right)^2} \approx (1 + i)\kappa^{1/2} \qquad (A.2)$$

Using eq A.2, the Fresnel's coefficient can be approximated as

$$L_T(\beta_c^0) = \frac{2n_1 \cos(\beta_c^0)}{n_2'(1 + i\kappa)\cos(\beta_c^0) + n_1 \cos(\gamma)}$$

$$\approx \frac{2n_1 \cos(\beta_c^0)}{n_2' \cos(\beta_c^0) + n_1\kappa^{1/2} + i(n_2'\kappa \cos(\beta_c^0) + n_1\kappa^{1/2})} \qquad (A.3)$$

It follows that

$$|L_T(\beta_c^0)|^2 = \frac{4n_1^2 \cos^2(\beta_c^0)}{(n_2' \cos(\beta_c^0) + n_1\kappa^{1/2})^2 + (n_2'\kappa \cos(\beta_c^0) + n_1\kappa^{1/2})^2}$$

$$< \left(\frac{2n_1}{n_2' + n_1\kappa^{1/2}/\cos(\beta_c^0)}\right)^2$$

$$= \left(\frac{2n_1}{n_2' + n_1\kappa^{1/2}(1 - \sin^2(\beta_c^0))^{-1/2}}\right)^2$$

$$= \left(\frac{2}{n}\right)^2 \left(\frac{1}{1 + n^{-1}(1 - n^2)^{-1/2}\kappa^{1/2}}\right)^2 \qquad (A.4)$$

where $n = \sin(\beta_c^0) = n_2'/n_1$. In the derivation of eq A.4, we neglected the term $(n_2'\kappa \cos(\beta_c^0) + n_1\kappa^{1/2})^2$ in the denominator since this term is small due to the assumption $\kappa \ll 1$. Furthermore, this term is greater than zero, so we obtain the inequality after neglecting this term in the denominator. In eq A.4, $(2/n)^2$ is the maximum of $|L_T(\beta)|^2$ in the case of $\kappa = 0$, and $(1/1 + n^{-1}(1 - n^2)^{-1/2}\kappa^{1/2})^2$ is a factor that shows how the increase of κ can lower the value of $|L_T(\beta)|^2$. For example, let the imaginary part of n_2 be 9% of the real part, that is, $\kappa = 0.09$, and let $n = n_2'/n_1 = 1.34/1.46 = 0.92$, then

$$n^{-1}(1 - n^2)^{-1/2} = 0.92^{-1}(1 - 0.92^2)^{-1/2} = 2.8, \kappa^{1/2} = 0.3,$$
$$\left(\frac{1}{1 + n^{-1}(1 - n^2)^{-1/2}\kappa^{1/2}}\right)^2 = \left(\frac{1}{1 + 2.8 \times 0.3}\right)^2 = \frac{1}{3.4} \qquad (A.5)$$

Equation A.5 shows that, even with $\kappa = 0.09$, the maximum of $|L_T(\beta)|^2$ drops to less than one-third of its maximum at $k = 0$. The fact that $|L_T(\beta)|^2$ decreases so quickly is because the square root taken on κ amplifies the effect of a small κ, the real part n_2' of n_2 is close to n_1, and $n^{-1}(1 - n^2)^{-1/2}$ becomes large as n becomes close to l.

From the above analysis, we can conclude that, in our near TIR geometry, the transmitted IR electric field can be depressed by the imaginary part of the water refractive index. Because of the frequency dependence of the index of refraction of water, the transmitted IR electric field is frequency dependent. The fact that the real part of the water refractive index is close to the silica refractive index further amplifies the effect caused by the imaginary part of the refractive index on the transmitted IR electric field. *The above analysis can be repeated if n_1 is a complex value and n_2 is real*. The general observation is the same: if the imaginary part of n_1 is nonzero, the enhancement at the critical angle is much less (Figure A.2).

It is of interest to explore the more general case where $n_1 = n_1'(1 + i\kappa_1)$ and $n_2 = n_2'(1 + i\kappa_2)$ are both complex. Figure A.3 shows the Fresnel coefficient at the critical angle, $|L_T(\beta_c^0)|^2$, as a function of $\kappa_2 - \kappa_1$ and $(\kappa_1 + \kappa_2)/2$. This result indicates that the enhancement purely depends on the difference $|\kappa_2 - \kappa_1|$. If $\kappa_1 = \kappa_2$, the enhancement is maximized. The enhancement decreases very fast as $|\kappa_2 - \kappa_1|$ increases. When $|\kappa_2 - \kappa_1| = 0.1$, the enhancement is less than 25% of its maximal value.

Acknowledgment. This work was supported by the Director, Office of Science, Office of Basic Energy Sciences, Materials Sciences and Engineering Division of the U.S. Department of Energy under Contract No. DE-AC02-05CH11231. Additional support was provided by the NIH through grant R21EB005262. We would like to thank Dr. Sasha J. Kweskin for inspiration to experiment with TIR-SFG and Prof. Yuen-Ron Shen for numerous discussions.

References and Notes

(1) Hunt, J. H.; Guyot-Sionnest, P.; Shen, Y. R. *Chem. Phys. Lett.* **1987**, *133*, 189–192.
(2) Zhu, X. D.; Suhr, H.; Shen, Y. R. *Phys. Rev. B* **1987**, *35*, 3047–3050.
(3) Harris, A. L.; Chidsey, C. E. D.; Levinos, N. J.; Loiacono, D. N. *Chem. Phys. Lett.* **1987**, *141*, 350–356.
(4) Shen, Y. R. *Nature* **1989**, *337*, 519–525.
(5) Shen, Y. R. *Solid State Commun.* **1997**, *102*, 221–229.
(6) Miranda, P. B.; Shen, Y. R. *J. Phys. Chem. B* **1999**, *103*, 3292–3307.
(7) Gracias, D. H.; Chen, Z.; Shen, Y. R.; Somorjai, G. A. *Acc. Chem. Res.* **1999**, *32*, 930–940.
(8) Chen, Z.; Shen, Y. R.; Somorjai, G. A. *Annu. Rev. Phys. Chem.* **2002**, *53*, 437–465.
(9) Raschke, M. B.; Shen, Y. R. *Curr. Opin. Solid State Mater. Sci.* **2004**, *8*, 343–352.
(10) Shen, Y. R.; Ostroverkhov, V. *Chem. Rev.* **2006**, *106*, 1140–1154.
(11) Eisenthal, K. B. *Annu. Rev. Phys. Chem.* **1992**, *43*, 627–661.
(12) Eisenthal, K. B. *Chem. Rev.* **1996**, *96*, 1343–1360.
(13) Bain, C. D. *Curr. Opin. Colloid Interface Sci.* **1998**, *3*, 287–292.
(14) Somorjai, G. A.; Rupprechter, G. *J. Phys. Chem. B* **1999**, *103*, 1623–1638.
(15) Shultz, M. J.; Schnitzer, C.; Simonelli, D.; Baldelli, S. *Int. Rev. Phys. Chem.* **2000**, *19*, 123–153.
(16) Somorjai, G. A.; McCrea, K. R. *Adv. Catal.* **2000**, *45*, 385–438.
(17) Allen, H. C.; Raymond, E. A.; Richmond, G. L. *Curr. Opin. Colloid Interface Sci.* **2000**, *5*, 74–80.
(18) Richmond, G. L. *Annu. Rev. Phys. Chem.* **2001**, *52*, 147–162.
(19) Buck, M.; Himmelhaus, M. *J. Vac. Sci. Technol. A* **2001**, *19*, 966–986.
(20) Schultz, M. J.; Baldelli, S.; Schnitzer, C.; Simonelli, D. *J. Phys. Chem. B* **2002**, *106*, 5313–5324.
(21) Richmond, G. L. *Chem. Rev.* **2002**, *102*, 2693–2724.
(22) Koffas, T. S.; Amitay-Sadovsky, E.; Kim, J.; Somorjai, G. A. *J. Biomater. Sci., Polym. Ed.* **2004**, *15*, 475–509.
(23) Opdahl, A.; Koffas, T. S.; Amitay-Sadovsky, E.; Kim, J.; Somorjai, G. A. *J. Phys., Condens. Matter* **2004**, *16*, R659−R677.
(24) Chen, X. Y.; Clarke, M. L.; Wang, J.; Chen, Z. *Int. J. Modern Phys. B* **2005**, *19*, 691–713.
(25) Lambert, A. G.; Davies, P. B.; Neivandt, D. J. *Appl. Spectrosc. Rev.* **2005**, *40*, 103–145.
(26) Vidal, F.; Tadjeddine, A. *Rep. Prog. Phys.* **2005**, *68*, 1095–1127.
(27) Wang, H. F.; Gan, W.; Lu, R.; Rao, Y.; Wu, B. H. *Int. Rev. Phys. Chem.* **2005**, *24*, 191–256.
(28) Gopalakrishnan, S.; Liu, D. F.; Allen, H. C.; Kuo, M.; Schultz, M. J. *Chem. Rev.* **2006**, *106*, 1155–1175.

(29) Hopkins, A. J.; McFearin, C. L.; Richmond, G. L. *Curr. Opin. Solid State Mater. Sci.* **2006**, *9*, 19–27.
(30) Chen, X. Y.; Chen, Z. *Biochim. Biophys. Acta, Biomembr.* **2006**, *1758*, 1257–1273.
(31) Ma, G.; Allen, H. C. *Photochem. Photobiol.* **2006**, *82*, 1517–1529.
(32) Kubota, J.; Domen, K. *Anal. Bioanal. Chem.* **2007**, *388*, 17–27.
(33) Chen, Z. *Polym. Int.* **2007**, *56*, 577–587.
(34) Wampler, R. D.; Moad, A. J.; Moad, C. W.; Heiland, R.; Simpson, G. J. *Acc. Chem. Res.* **2007**, *40*, 953–960.
(35) Baldelli, S. *Acc. Chem. Res.* **2008**, *41*, 421–431.
(36) York, R. L.; Browne, W. K.; Geissler, P. L.; Somorjai, G. A. *Isr. J. Chem.* **2007**, *47*, 51–58.
(37) Hatch, S. R.; Polizzotti, R. S.; Dougal, S.; Rabinowitz, P. *Chem. Phys. Lett.* **1992**, *196*, 97–102.
(38) Conboy, J. C.; Messmer, M. C.; Richmond, G. L. *J. Phys. Chem.* **1996**, *100*, 7617–7622.
(39) Conboy, J. C.; Messmer, M. C.; Richmond, G. L. *J. Phys. Chem. B* **1997**, *101*, 6724–6733.
(40) Lobau, J.; Wolfrum, K. *J. Opt. Soc. Am. B, Opt. Phys.* **1997**, *14*, 2502–2512.
(41) Lobau, J.; Wolfrum, K. *Laser Phys.* **1998**, *8*, 582–592.
(42) Williams, C. T.; Yang, Y.; Bain, C. D. *Langmuir* **2000**, *16*, 2343–2350.
(43) Hatch, S. R.; Polizzotti, R. S.; Dougal, S.; Rabinowitz, P. *J. Vac. Sci. Technol. A: Vac. Surf. Films* **1993**, *11*, 2232–2238.
(44) Yang, Y. J.; Pizzolatto, R. L.; Messmer, M. C. *J. Opt. Soc. Am. B: Opt. Phys.* **2000**, *17*, 638–645.
(45) Gautam, K. S.; Schwab, A. D.; Dhinojwala, A.; Zhang, D.; Dougal, S. M.; Yeganeh, M. S. *Phys. Rev. Lett.* **2000**, *85*, 3854–3857.
(46) Nishi, N.; Hobara, D.; Yamamoto, M.; Kakiuchi, T. *Anal. Sci.* **2003**, *19*, 887–890.
(47) Harp, G. P.; Rangwalla, H.; Yeganeh, M. S.; Dhinojwala, A. *J. Am. Chem. Soc.* **2003**, *125*, 11283–11290.
(48) Knock, M. M.; Bell, G. R.; Hill, E. K.; Turner, H. J.; Bain, C. D. *J. Phys. Chem. B* **2003**, *107*, 10801–10814.
(49) Strunk, M. R.; Williams, C. T. *Langmuir* **2003**, *19*, 9210–9215.
(50) Rangwalla, H.; Dhinojwala, A. *J. Adhes.* **2004**, *80*, 37–59.
(51) Dreesen, L.; Sartenaer, Y.; Humbert, C.; Mani, A. A.; Lemaire, J. J.; Methivier, C.; Pradier, C. M.; Thiry, P. A.; Peremans, A. *Thin Solid Films* **2004**, *464*, 373–378.
(52) Kweskin, S. J.; Komvopoulos, K.; Somorjai, G. A. *Langmuir* **2005**, *21*, 3647–3652.
(53) Yeganeh, M. S.; Dougal, S. A.; Silbernagel, B. G. *Langmuir* **2006**, *22*, 637–641.
(54) Kweskin, S. J.; Rioux, R. M.; Habas, S. E.; Komvopoulos, K.; Yang, P.; Somorjai, G. A. *J. Phys. Chem. B* **2006**, *110*, 15920–15925.
(55) Wang, J.; Even, M. A.; Chen, X. Y.; Schmaier, A. H.; Waite, J. H.; Chen, Z. *J. Am. Chem. Soc.* **2003**, *125*, 9914–9915.
(56) Chen, X. Y.; Wang, J.; Sniadecki, J. J.; Even, M. A.; Chen, Z. *Langmuir* **2005**, *21*, 2662–2664.
(57) Wang, J.; Chen, X. Y.; Clarke, M. L.; Chen, Z. *Proc. Natl. Acad. Sci. U.S.A.* **2005**, *102*, 4978–4983.
(58) Downing, H. D.; Williams, D. *J. Geophys. Res.* **1975**, *80*, 1656–1661.
(59) Nihonyanagi, S.; Ye, K.; Uosaki, K. *Electrochemica Acta* **2001**, *46*, 3057–3061.
(60) Bloembergen, N.; Pershan, P. S. *Phys. Rev.* **1962**, *128*, 606–622.
(61) Heinz, T. F. University of California, Berkeley, 1982.
(62) Briggman, K. A.; Stephenson, J. C.; Wallace, W. E.; Richter, L. J. *J. Phys. Chem. B* **2001**, *105*, 2785–2791.
(63) Hopkins, A. J.; McFearin, C. L.; Richmond, G. L. *Curr. Opin. Solid State Mater. Sci.* **2005**, *9*, 19–27.

JP808629R